Hindawi
Journal of Electrical and Computer Engineering
Volume 2023, Article ID 8931693, 11 pages
https://doi.org/10.1155/2023/8931693

Research Article

Material Characteristics and Electrical Performance of Perovskite Solar Cells with Different Carbon-Based Electrodes Mixed with CuSCN

Elang Barruna, Atya Saniah, Siti Fauziyah Rahman, and Nji Raden Poespawati

Department of Electrical Engineering, Faculty of Engineering, Universitas Indonesia, Depok 16242, Indonesia

Correspondence should be addressed to Nji Raden Poespawati; pupu@eng.ui.ac.id

Received 21 March 2023; Revised 5 May 2023; Accepted 17 May 2023; Published 28 June 2023

Academic Editor: Mohamed Louzazni

Perovskite solar cells are the most cutting-edge photovoltaic technology having high efficiency and short fabrication time. In recent decades, there has been a significant rise in the study of the usage of carbon materials in perovskite solar cells because of low cost and earth abundance. Several studies have been conducted to mix hole transport materials with carbon materials to improve the hole extraction capability. Nevertheless, no research has reported using CuSCN on different carbon electrodes on perovskite solar cells. In this research, various carbon materials, including carbon nanotubes (CNT), graphite, activated carbon, and reduced graphene oxide (rGO), are mixed with CuSCN. The carbon materials and CuSCN were mixed by ball mill and then deposited using the doctor blading method to become an electrode layer. The existence of CuSCN in carbon materials was proved by conducting the energy dispersive X-ray test. CNT mixed with CuSCN material exhibits the highest electrical conductivity indicated by I_D/I_G ratio of 1.22 using Raman spectroscopy. Perovskite solar cell with a mix of CNT and CuSCN electrode exhibits the lowest series resistance of 76.69 Ω, resulting in the optimum solar cell performance such as a short-circuit current density (J_{SC}) of 0.199 mA/cm^2, open-circuit voltage (V_{OC}) of 0.52 V, fill-factor (FF) of 0.369, and efficiency of 0.0735.

1. Introduction

The development of photovoltaics began with the introduction of the first generation of photovoltaics using silicon material founded by Bell Labs in 1954. Even though the efficiency of silicon solar cells is relatively high at 25%, this solar cell production is relatively expensive and complex [1]. After that, the second generation of photovoltaics emerged, thin-film solar cells. Though thin-film solar cells can be produced more efficiently and have lower production costs, second-generation solar cells' efficiency is not greater than that of the first generation. Therefore, the third generation emerged, namely, perovskite solar cells, which meet the record efficiency and short fabrication time [2].

Perovskite solar cells (PSCs) have an active layer made of perovskite. Perovskite materials have attracted a lot of attention because they can be implemented in several applications, such as solar cells [3], energy storage devices [4], and light-emitting diodes [5]. Perovskite is a material discovered by Russian mineralogist L. A. Perovski with an ABX_3 crystal structure. An organic cation, such as methylammonium (MA) and formamidinium (FA), is denoted by the letter A. B is a metal cation, such as lead (Pb^{2+}), tin (Sn^{2+}), and germanium ($Ge2^{+}$). The halide anion (X) includes iodine (I^{-}), bromine (Br^{-}), and chlorine (Cl^{-}) [6]. PSCs were first discovered by Akihiro Kojima in 2009 with an efficiency of 3.8% and rocketed to 25% in 2022 [7, 8]. People are giving a lot of attention to perovskite solar cells because of their low-priced production, easy manufacturing, and high efficiency [9].

Although the rise in the efficiency value of perovskite solar cells is accelerating, some challenges must be addressed, such as stability and upscaling [10]. In recent decades, there has been a significant rise in the study of the usage of carbon materials in PSCs [11]. Carbon materials have the potential to be applied to PSCs because of their

superior characteristics, namely, low cost and earth abundance [12, 13]. Carbon materials can be inserted into various layers of perovskite solar cells, such as the electrode layer, hole transport layer (HTL), perovskite layer, and electron transport layer (ETL) [14].

Several reports have revealed that perovskite solar cells with carbon-based electrodes can produce good stability [15] and withstand moisture [16]. Ku et al. originally proposed using carbon materials in perovskite solar cells in 2013. They used the deposition printing technique to apply carbon material to the counter electrode of PSCs [17]. Along with the developing solar cell technology, perovskite solar cells with carbon counter electrodes are also known as carbon-perovskite solar cells (C-PSCs) [18].

Eliminating HTL in perovskite solar cells can enhance stability, reduce costs, and simplify fabrication [19]. However, several unresolved issues exist because of the absence of HTL, such as bad surface contact between the electrode layer and the perovskite layer, ineffective hole mobility, and a mismatch of energy level arrangements [20]. Therefore, mixing hole transport material (HTM) and carbon on perovskite solar cell electrodes is a potential effort to improve the hole extraction capability due to the shorter charge transport path [21]. Ball milling is a mixing technique that is ecofriendly and reliable [22]. Several studies have been conducted to mix carbon with HTM, such as adding CuS [23] and CuPc [24] in carbon black and graphite counter electrodes of PSCs. However, no research has reported the performance of perovskite solar cells when affected by the use of CuSCN on various carbon electrodes. CuSCN is used because it is an HTM having the highest conduction band energy level [25].

In this research, we investigate the effect of using various carbon materials, including carbon nanotubes (CNTs), graphite, activated carbon, and reduced graphene oxide mixed with CuSCN-based HTM at the counter electrode on the material characteristics and the performance of perovskite solar cells.

2. Materials and Methods

2.1. Device Architecture. The perovskite solar cell structure is illustrated in Figure 1. It uses the n-i-p architecture. FTO-coated glass (Sigma-Aldrich) is applied as a top contact of perovskite solar cells because of its good characteristics, including high transparency, low sheet resistance, and easy deposition [26]. We used TiO_2 (Sigma-Aldrich) as the electron transport material (ETM) because it has several excellent properties, such as a large band gap (3.7 eV), good optical transparency, good electron mobility, and good environmental stability [25].

For the active layer, chlorine-based perovskite material ($CH_3NH_3PbCl_3$) from Sigma-Aldrich is used due to its good properties, namely, the high light absorption coefficient, good electron transport characteristics, and good stability [25, 27]. The counter electrode consists of two materials, namely, HTM and carbon. For the HTM, we used CuSCN due to its outstanding characteristics, namely, high hole mobility, good chemical stability, broad band gap (3.8 eV),

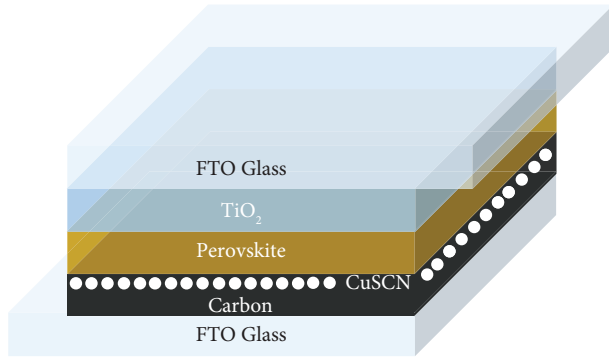

Figure 1: Perovskite solar cell structure.

and high energy level of the conduction band [27, 28]. For the carbon, we used activated carbon provided by Megah Abadi Chemical, graphite and carbon nanotubes (CNTs) from Sigma-Aldrich, and reduced graphene oxide (rGO), which was synthesized by using Hummer and chemical reduction methods. Lastly, the cell's rear contact is made of FTO-coated glass.

In perovskite solar cells, the mobility of electrons and holes explains how the device works. The movement of electrons and holes can be described by using an energy level diagram. Figure 2 illustrates a representation of the energy levels of the manufactured perovskite solar cells. The energy level of FTO-coated glass is −4.4 eV [29]. The valence and conduction energy levels for TiO_2 are −8.0 eV and −4.3 eV, respectively [25]. The energy levels of both valence and conduction bands of the perovskite layer are −5.43 eV and −3.75 eV [27]. The proposed devices have a counter electrode made of CuSCN and carbon, which causes a 0.2 eV energy shift [24]. As a result, the electrode with a mixture of carbon and CuSCN has valence and conduction energy levels of −5.1 eV and −1.3 eV [20, 25].

2.2. Reduced Graphene Oxide Synthesis. This research synthesizes graphene material from graphite powder with Hummer and chemical reduction methods. Generally, oxidation and reduction are two essential processes in synthesizing reduced graphene oxide (rGO) [30, 31].

The oxidation process is carried out to create graphene oxide (GO) from graphite powder. First, 3 g of graphite powder and 1.5 g of $NaNO_3$ are dispersed in 69 ml of H_2SO_4 and stirred while sitting on an ice bath with a solution temperature of 10°C. After that, 9 g of $KMNO_4$ were added while maintaining the temperature below 20°C. Once the mixture had been heated to 35°C and stirred for 30 minutes, 138 ml of water was added and maintained at 67°C for 15 minutes. Then, the mixture was rinsed with 200 ml of HCl, distilled water, and ethanol, followed by a filtering process. After that, the mixture was then heated at a temperature of 70°C for 24 hours [32].

The reduction process begins with dissolving 10 g of ascorbic acid and 0.25 g of GO into 100 ml of aquadest. Then, the combination was heated at 95°C for 60 minutes and ultrasonicated for 900 seconds. After that, the mixture was twice rinsed in 200 ml of distilled water and ethanol,

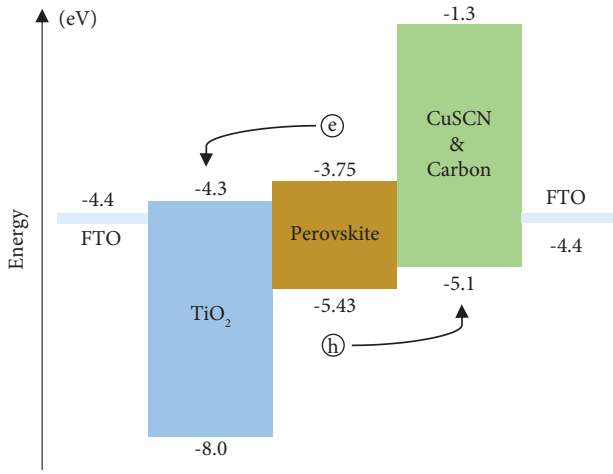

Figure 2: The energy level arrangement in a perovskite solar cell.

followed by a filtering process. Once the mixture had been filtered, it was then heated at a temperature of 70°C for 24 hours until reduced graphene oxide (rGO) was obtained [32].

2.3. Preparation of Precursors and Carbon Paste. TiO_2 precursor, perovskite precursor, and carbon paste should be prepared before the fabrication process. In the process of making TiO_2 precursor, 0.3 ml of titanium (IV) isopropoxide (TTIP) was mixed with 0.1 ml of hydrochloric acid (HCl) and 5 ml of ethanol (C_2H_6O). After that, the precursor was stirred for 15 minutes at ambient temperature. Besides, the process of making perovskite precursor begins with mixing 240 mg of CH_3NH_3I powder, 140 mg of lead (II) chloride ($PbCl_2$) powder, and 1 ml of N, N-dimethylformamide (DMF) in a vial. Then, it was stirred for 60 minutes at a temperature of 80°C with a rotating speed of 800 rpm. Materials used in TiO_2 and perovskite precursors are obtained from Sigma-Aldrich.

The carbon paste comprises several materials, such as carbon powder, CuSCN, ethyl cellulose, and chlorobenzene. In this research, the carbon materials used are activated carbon derived from coconut shells, graphite, carbon nanotubes (CNTs), and reduced graphene oxide (rGO). The first step in making carbon paste is mixing 1 g of carbon material with 0.1 g of CuSCN [33] and 0.1 g of ethyl cellulose in a ball mill jar and stirring with a ball milling machine for 30 minutes. The ball milling technique was used because it effectively prepares materials with a large surface area, such as carbon [34, 35]. Subsequently, the mixed carbon powder was dissolved in 0.3 ml of C_6H_5Cl (chlorobenzene) until it became a carbon paste.

2.4. Device Fabrication. Figure 3 explains the procedure of fabrication of carbon-based electrode perovskite solar cells. Before the perovskite solar cell fabrication process is carried out, there is a stage called precleaning. Precleaning is a stage that involves using an ultrasonic cleaner to wash FTO glass in distilled water, acetone, and ethanol for five minutes. The first stage in the device fabrication process is TiO_2 deposition. On top of the cleaned FTO glass, a drop of a TiO_2 precursor was placed, and then it was spin coated for half a minute at a speed rate of 2000 rpm. After that, the deposited TiO_2 layer was annealed at a temperature of 425°C for half an hour.

The next stage is perovskite deposition by dripping 0.13 ml of perovskite precursor onto the FTO glass deposited with TiO_2. Then, it was spin coated for 30 seconds with a rotating speed of 1000 rpm. Subsequently, it was annealed at a temperature of 130°C for 15 minutes, as shown in Figure 4(a). Afterwards, the carbon paste was deposited on a cleaned FTO glass using the doctor blading method, often used to deposit carbon materials [25]. Then, it was annealed at a temperature of 100°C for twenty minutes, as shown in Figure 4(b). The final step is assembling two half cells by clips into a complete solar cell having an active area of 2.25 cm^2.

2.5. Material Characterization and Photovoltaic Parameter Measurement. Material characteristics of the carbon-based electrode, such as surface morphology, element composition, and element distribution, were measured by scanning electron microscopy (SEM), energy dispersive X-ray (EDX), and EDX mapping using the ZEISS EVO MA 10 with a magnification of 1000. In addition, the carbon structure was investigated by Raman spectroscopy (Bruker). In order to determine the *D* and *G* bands' peak values, the Raman spectra were deconvoluted using the Gaussian function [36].

The fabricated devices were measured by the HP 4145B semiconductor parameter analyzer in a dark condition to obtain the dark I-V curve. After that, they were placed outdoors and got direct sunlight. The intensity of sunlight was measured using a solar power meter. A multimeter measured the generated current (I_L). The dark I-V curve was subtracted by the I_L using equation (1) to shift downward [27].

$$I = I_o\left[\exp\left(\frac{qV}{kT}\right) - 1\right] - I_L, \tag{1}$$

$$\mathrm{FF} = \frac{V_{\mathrm{MP}} \times I_{\mathrm{MP}}}{V_{\mathrm{OC}} \times I_{\mathrm{SC}}}, \tag{2}$$

$$\eta = \frac{V_{\mathrm{OC}} \times I_{\mathrm{SC}} \times \mathrm{FF}}{P_{\mathrm{in}}} \times 100\%. \tag{3}$$

The shifted dark I-V curve was then rotated on the *x*-axis, becoming a typical I-V curve. The I-V curve can show the short circuit current (I_{SC}), open circuit voltage (V_{OC}), maximum power voltage (V_{MP}), and maximum power current (I_{MP}). The fill factor (FF) was calculated using equation (2). Furthermore, the efficiency was calculated using equation (3) [27]. The resistance measurement was carried out using the PalmSens, EmStat4S. The Randles equivalent circuit was used in the resistance measurement connecting the series resistance (R_s) in series and the transfer resistance (R_{trans}) as well as recombination resistance (R_{rec})

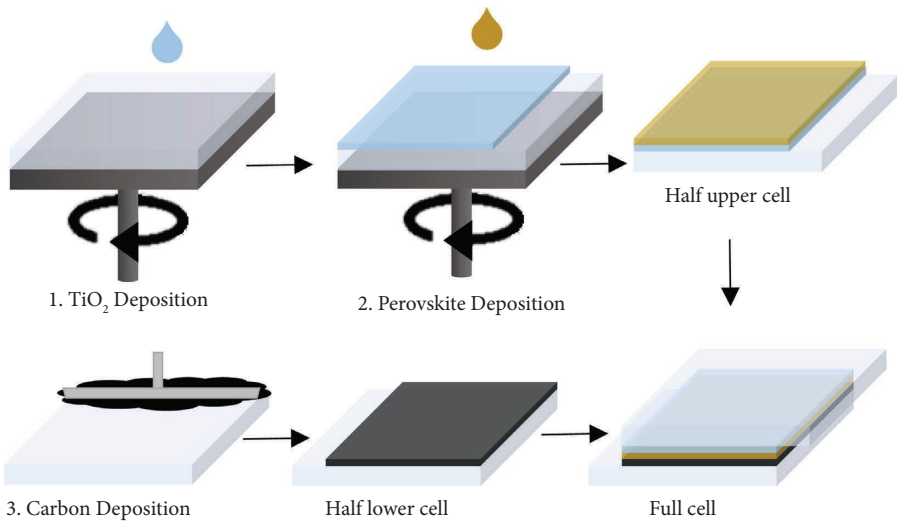

Figure 3: Carbon-based electrode perovskite solar cell fabrication procedure.

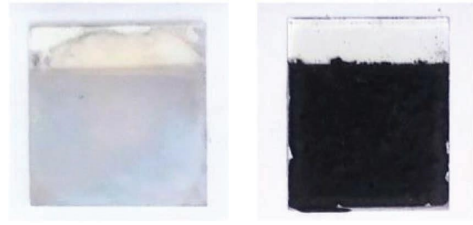

Figure 4: Deposited layer of (a) TiO_2/perovskite and (b) combined CuSCN and carbon.

in parallel, as shown in Figure 5. The R_s, R_{trans}, and R_{rec} are values that represent the phenomenon of charge transport in carbon, perovskite, and electron transport layers.

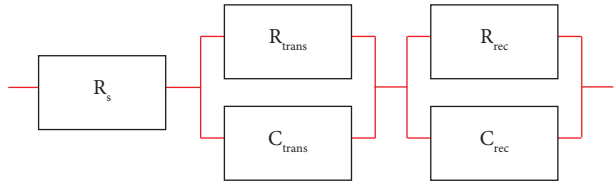

Figure 5: Randles equivalent circuit.

3. Results and Discussion

3.1. Surface Morphology. The surface morphology of each carbon material deposited on the FTO glass can be seen in Figures 6(a)–6(f). Figure 6(a) shows the bare activated carbon, while Figure 6(b) represents the combined activated carbon and CuSCN. Both Figures 6(a) and 6(b) illustrate that electrodes made from activated carbon have particles that are random orientation and bulky [37, 38]. Figure 6(c) describes that CNTs have a one-dimensional structure with a shape like a very long cylindrical tube and can cross one another [39]. Therefore, this structure can provide a high-speed transportation route, speeding up the charge transport process [40]. Figure 6(d) shows that graphite-based electrodes have a surface morphology like carbon sheets stacked on each other or often referred to as flaky graphite [21].

Figure 6(e) illustrates the surface morphology of graphene oxide (GO), and Figure 6(f) shows the surface morphology of reduced graphene oxide (rGO). Figures 6(e) and 6(f) illustrate that the surface of the electrode made from graphene-derived carbon has a smoother and more even surface. Therefore, the contact surface area between the electrode layer and the electrode layer in contact becomes larger [12].

3.2. Element Composition. Table 1 shows the elemental composition data for each electrode with variations in the carbon material used. The sample without CuSCN contains only 92.5% carbon and 7.5% oxygen and does not contain copper. On the contrary, the mixture of CuSCN and activated carbon has a carbon content of 91.87% and a copper content of 1.08%, indicating that the two materials' mixing process has been successfully carried out.

Electrodes made from CNT have a carbon content of 93.63% and a copper content of 2.26%. Graphite electrodes have a percentage of 91.77% carbon and 2.66% copper. The GO electrode has a carbon content of 63.8% and 19.57% oxygen. An electrode made of rGO has a carbon content of 65.86% and an oxygen content of

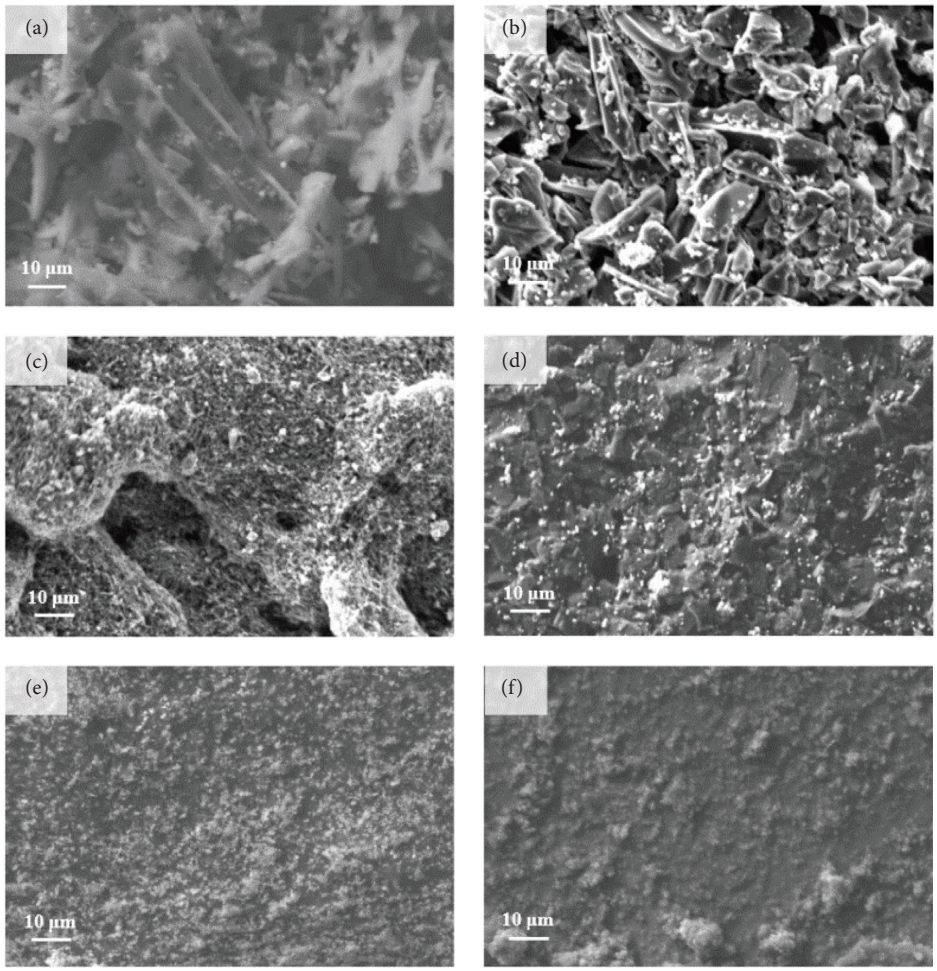

Figure 6: Surface morphology of the electrode made of (a) pure activated carbon, (b) activated carbon and CuSCN, (c) CNT and CuSCN, (d) graphite and CuSCN, (e) graphene oxide and CuSCN, and (f) reduced graphene oxide and CuSCN.

Table 1: Compositions of the CuSN-incorporated electrode with different carbons.

Electrode materials	Carbon (wt. %)	Oxygen (wt. %)	Copper (wt. %)
Bare activated carbon	92.50	7.50	0.00
CuSCN and activated carbon	91.87	2.79	1.08
CuSCN and CNT	93.63	1.82	2.26
CuSCN and graphite	91.77	3.03	2.66
CuSCN and GO	63.80	19.57	11.58
CuSCN and rGO	65.86	13.97	13.14

13.97%. An electrode made of rGO has a lower oxygen content than GO. This result indicates that the rGO synthesis process has succeeded in reducing the oxygen content. The oxidation method is the Hummer method because it is the most commonly used, safest, and fastest method [41, 42]. However, the Hummer method has a drawback; the ratio of carbon to oxygen content that can be produced is only 2.25 [43]. Therefore, the carbon content produced is not larger than 70%.

3.3. Element Distribution. Figures 7(a)–7(f) illustrate the distribution of elements for each electrode with variations in carbon materials. The copper (Cu) element can be illustrated in red, while carbon (C) is green. Based on Figure 7(a), the electrode made from pure activated carbon shows the absence of the element Cu in the carbon.

On the other hand, based on Figures 7(b)–7(d), the electrode consisting of a combination of CuSCN with activated carbon, CNT, and graphite showed the presence of

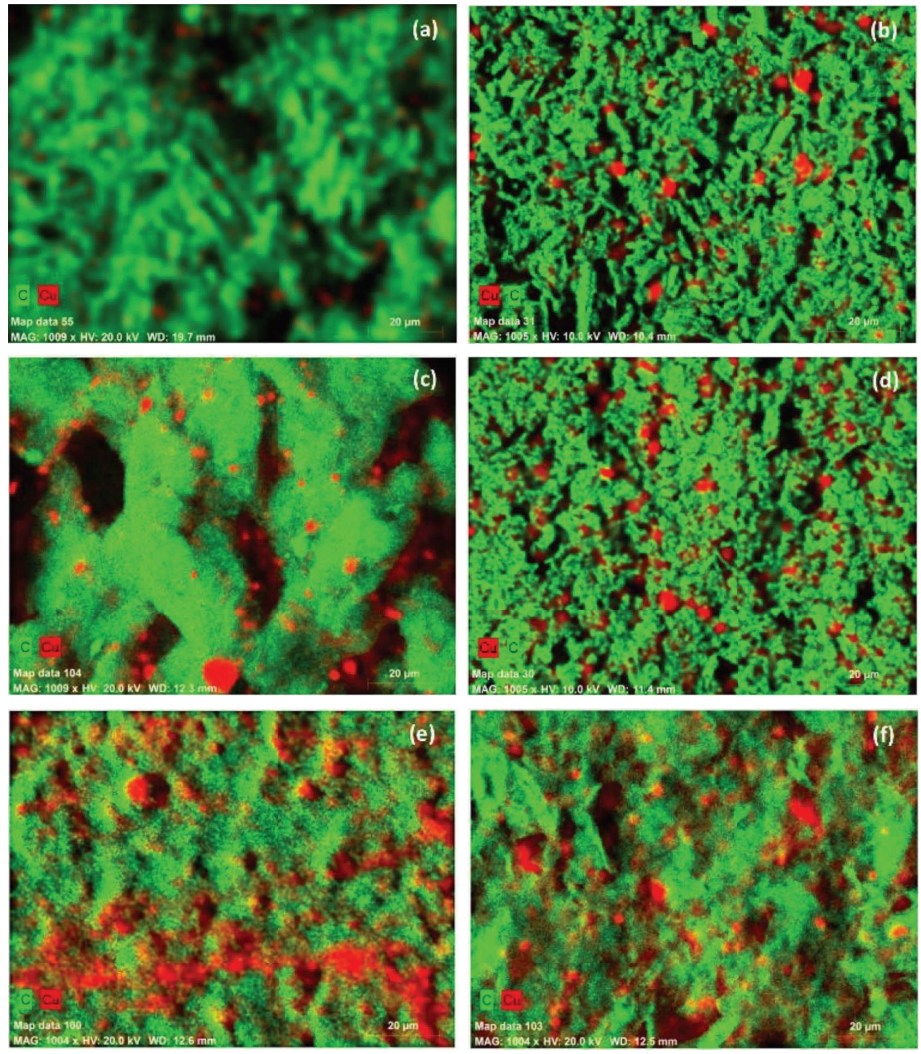

Figure 7: Carbon and copper distribution on the electrode made of (a) pure activated carbon, (b) activated carbon and CuSCN, (c) CNT and CuSCN, (d) graphite and CuSCN, (e) graphene oxide and CuSCN, and (f) reduced graphene oxide and CuSCN.

Cu on several sides of the carbon element. This result proves that the effort of mixing carbon and CuSCN materials on an electrode has been successfully carried out.

Based on Figure 7(e), the electrode made from GO and CuSCN illustrates the larger amount of element Cu in the element carbon. On the other hand, Figure 7(f) describes that the electrode made from a mixture of rGO and CuSCN shows a more dominant carbon element content. Based on these differences, it can be assumed that the reduction process during the rGO synthesis has succeeded in increasing carbon.

3.4. Carbon Structure Analysis. Raman spectroscopy is one of the most common methods for investigating carbonaceous materials [36]. In this work, the Raman shift was measured between 0 cm^{-1} and 3500 cm^{-1}. Generally, two common peaks in the Raman spectrum are D-band and G-band. While the D-band is located at around 1300 cm^{-1}, the G-band is located at around 1590 cm^{-1} [44]. D-band refers to the disordered graphitic material. This corresponds to the defective graphitic structure of carbon materials. G-band is attributed to the C-C bond in graphitic materials [45]. Figure 8 shows the Raman spectrum of different carbon materials.

Table 2 defines the I_D/I_G ratio of different carbon materials. The intensity ratio between D-band and G-band (I_D/I_G) was often measured to estimate the structural defect and structural quality of carbon materials [46, 47].

The CNT and CuSCN sample shows the highest I_D/I_G ratio value of 1.22, indicating it has many structural defects but has the best electrical conductivity properties. This happens because the higher the I_D/I_G ratio value, the higher the density of the structural defect of its sample [47]. However, it is inversely correlated with the electrical conductivity [45]. It is followed by GO and rGO samples producing I_D/I_G ratio values of 0.96 and 1.19. This trend definitely corresponds to the values reported by Suragtkhuu et al. [48]. The minor increase in the I_D/I_G ratio value from GO to rGO indicates that the defects are introduced to the sp2 carbon during the reduction process. Therefore, the reduction of GO is successfully conducted [49].

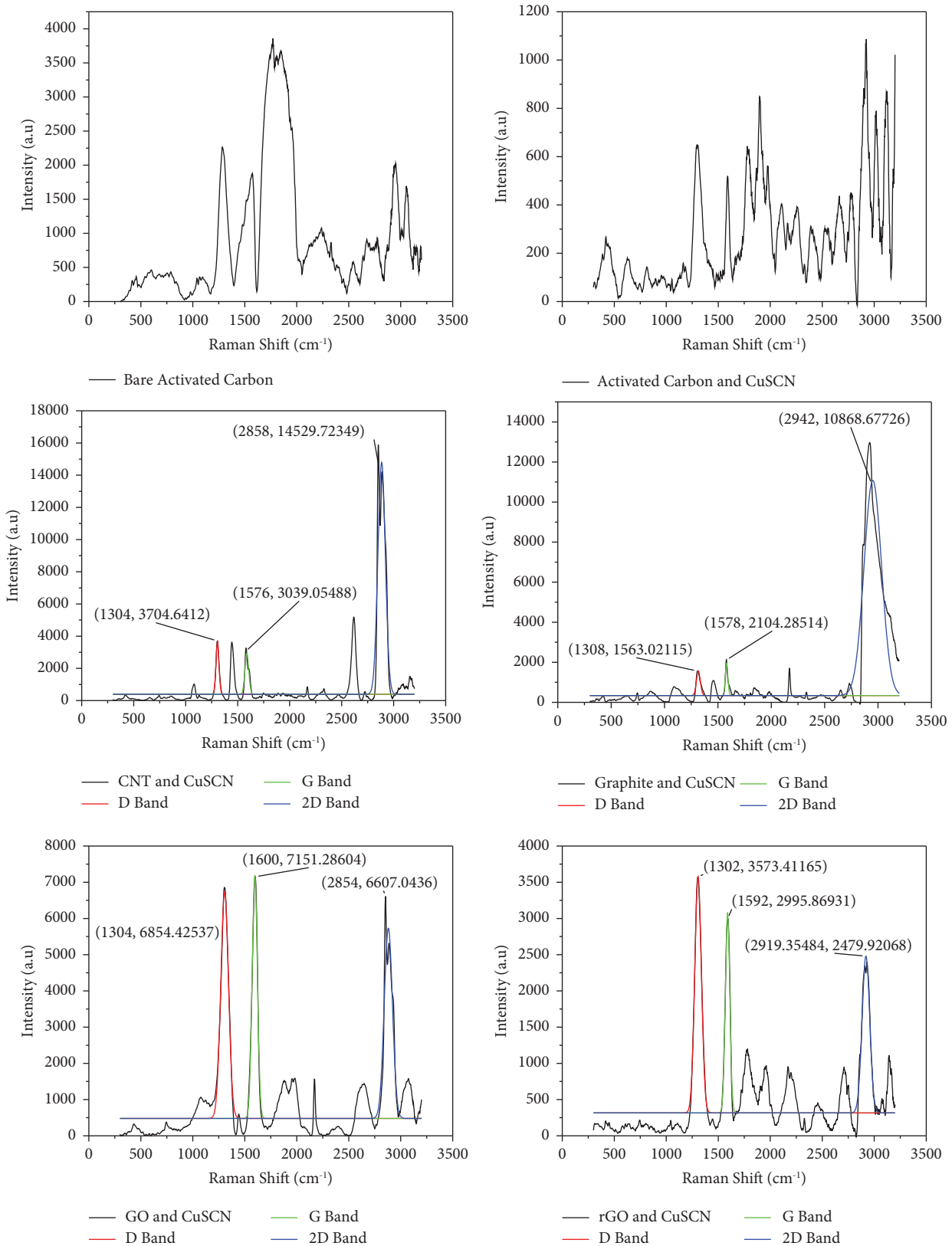

Figure 8: Raman original spectra and Gaussian-fitted spectra of different carbon materials.

Table 2: The I_D/I_G ratio of different mixed carbon materials.

Materials	I_D/I_G ratios
Bare activated carbon	—
CuSCN and activated carbon	—
CuSCN and CNT	1.22
CuSCN and graphite	0.74
CuSCN and GO	0.96
CuSCN and rGO	1.19

Graphite and CuSCN produce the lowest I_D/I_G ratio value of 0.94. This sample indicates the highest structural quality because the lower the I_D/I_G ratio value, the fewer the defects and the better the structural quality. However, it has the lowest electrical conductivity value.

3.5. Resistance Analysis. In general, resistance analysis is used to analyze the charge transport phenomenon that occurs in perovskite solar cells. The Randles circuit connects the series resistance (R_s) in series while the transfer resistance (R_{trans}) and recombination resistance (R_{rec}) are connected in parallel. Therefore, the analysis of R_s is opposite to that of R_{trans} and R_{rec}.

The R_s, R_{trans}, and R_{rec} shown in Table 3 are values that represent the phenomenon of charge transport in carbon, perovskite, and electron transport layers, respectively [50, 51]. There is no GO electrode because it is an insulator [52]. Therefore, it cannot be applied as an electrode.

Table 3 explains that the smallest series resistance value of 76.69 Ω is obtained from the device with a CNT and CuSCN electrode. Then, the device with an electrode made from pure activated carbon, a combination of CuSCN with activated carbon, graphite, and rGO, produced a series resistance of 283.4 Ω, 194.7 Ω, 633 Ω, and 50000 Ω, respectively. Perovskite solar cells with CNT and CuSCN-based electrodes produce the smallest R_s indicating that the charge movement from the perovskite to the carbon layer occurs effectively. This happens because CNT has a very high conductivity level compared to conventional carbons such as graphite [39, 53, 54]. Compared to R_{trans} and R_{rec}, R_s is the value affecting solar cell performance the most [55].

Perovskite solar cells with an electrode of pure activated carbon produced a R_{trans} value of 131.6 Ω. Furthermore, perovskite solar cells with an electrode made from a combination of CuSCN with activated carbon, CNT, graphite, and rGO produced a R_{trans} value of 82.48 Ω, 2322 Ω, 3415 Ω, and 0.000001 Ω, respectively. The low R_{trans} value indicates inefficient charge movement from the perovskite layer to the carbon layer [40]. This is because the perovskite layer's surface is of poor quality, which increases the probability that recombination will occur there [21].

PSCs with counter electrodes consisting of a mixture of CuSCN with CNT, graphite, and rGO produced R_{rec} values with insignificant differences, namely, 1372 Ω, 1138 Ω, and 1491 Ω, respectively. On the other side, PSCs with an electrode made of pure activated carbon and a mixture of activated carbon with CuSCN resulted in a R_{rec} of 1.09 Ω and 7.583 Ω. In contrast to the series resistance characteristics, the higher the R_{rec} value of a PSC, the lower the recombination that occurs in the PSC [56]. Therefore, the probability of recombination in the ETL layer of PSCs with counter electrodes consisting of a combination of CuSCN with CNT, graphite, and rGO is relatively low. On the other hand, the probability of recombination occurring in the ETL of perovskite solar cells with an electrode made of pure activated carbon and a combination of CuSCN and activated carbon is high.

Table 3: The value of resistances of PSCs with different electrode materials.

Electrode materials	R_s (Ω)	R_{trans} (Ω)	R_{rec} (Ω)
Bare activated carbon	283.4	131.6	1.090
CuSCN and activated carbon	194.7	82.48	7.583
CuSCN and CNT	76.69	2322	1372
CuSCN and graphite	633	3415	1138
CuSCN and rGO	50000	0.000001	1491

3.6. Device Performance. Table 4 explains the performance of perovskite solar cells with different electrode materials, such as short circuit current density (J_{SC}), open-circuit voltage (V_{OC}), and fill factor (FF), which were reprinted with permission from Barruna et al.'s study [57].

The highest short-circuit current of 0.199 mA/cm^2 was obtained from a perovskite solar cell with a counter electrode consisting of CNT and CuSCN due to several factors such as a high conductivity value of MWCNT (35.6 S/cm) [21], low value of R_s, and high value of both R_{trans} and R_{rec}. Perovskite solar cells with mixed electrodes of CuSCN with rGO, graphite, and activated carbon produced J_{SC} of 0.019 mA/cm^2, 0.070 mA/cm^2, and 0.000004 mA/cm^2, respectively. The small J_{SC} value is the result of the high value of Rs and the low values of both R_{trans} and $R_{rec,}$ illustrating the high recombination rate in the carbon, perovskite, and ETL layers sequentially [56].

The I-V curve of the fabricated perovskite solar cells with a variety of carbon materials is described in Figure 9. The perovskite solar cell having an electrode made of CNT and CuSCN produced the largest squareness. As a result, this device shows the largest FF of 0.369. Furthermore, perovskite solar cells with CuSCN mixed electrodes with graphite and rGO resulted in FF values of 0.348 and 0.273, respectively. The result in this research is supported by the research reported by Cai et al. stating that perovskite solar cells with an electrode made of MWCNT could produce the best FF value of 0.75 compared to carbon black and graphite electrodes showing FF values of 0.65 and 0.64 [58].

Based on the PCE values, the perovskite solar cell with a counter electrode made from a mixture of CNT and CuSCN produced the most significant efficiency of 0.0735%. Besides, the solar cells with an electrode made of graphite and CuSCN shows a PCE of 0.0168%. Lastly, the solar cell with an electrode made of rGO and CuSCN produced an efficiency of 0.0003%. Perovskite solar cell with an electrode made of CuSCN and CNT shows the highest efficiency because the V_{OC} and J_{SC} values of this cell are higher than the solar cells with an electrode made of graphite and rGO.

Overall, a perovskite solar cell with a counter electrode made of a mixture between CNT and CuSCN illustrates the best fill factor and efficiency. This result concurs with the

Table 4: Photovoltaic parameters of perovskite solar cells with different electrode materials.

Electrode materials	J_{sc} (mA/cm^2)	V_{oc} (V)	FF	η (%)
Bare activated carbon	0.000004	0	0	—
CuSCN and activated carbon	0.000004	0	0	—
CuSCN and CNT	0.199	0.52	0.369	0.0735
CuSCN and graphite	0.070	0.36	0.348	0.0168
CuSCN and rGO	0.019	0.06	0.273	0.0003

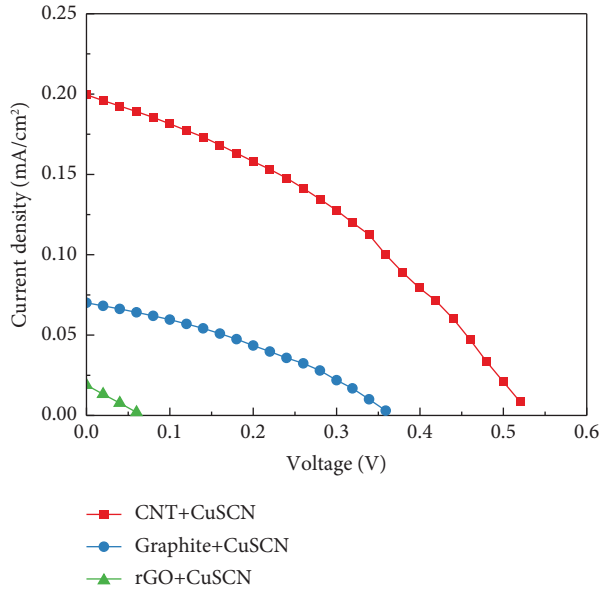

Figure 9: Current-voltage (I-V) curve of perovskite solar cells with different carbon electrode materials.

study reported by Wang et al. that mixing HTM with MWCNT-type carbon at the electrode layer can speed the charge mobility, decrease recombination, and boost conductivity; so, it can boost J_{sc} and results in a high fill factor and efficiency [56].

4. Conclusion

In conclusion, combining CuSCN-based HTM and several carbon materials such as activated carbon, graphite, CNT, and rGO on the electrode layer of a perovskite solar cell was demonstrated. CNT mixed with the CuSCN material exhibits the highest conductivity indicated by the I_D/I_G ratio value of 1.22. Based on the resistance measurement, the perovskite solar cell with a CNT-mixed CuSCN electrode has the lowest series resistance of 76.69 Ω, resulting in the optimum solar cell performance such as J_{SC} of 0.199 mA/cm^2, V_{OC} of 0.52 V, FF of 0.369, and efficiency of 0.0735%.

Data Availability

Data used to support the findings of this study are included within the article.

Conflicts of Interest

The authors declare that there are no conflicts of interest.

Acknowledgments

This study was funded by Hibah Publikasi Terindeks Internasional (PUTI) Pascasarjana, Tahun Anggaran 2022-2023, Nr. NKB-331/UN2.RST/HKP.05.00/2022.

References

[1] Y. Kuang, M. D. Vece, J. K. Rath, L. V. Dijk, and R. E. I. Schropp, "Elongated nanostructures for radial junction solar cells," *Reports on Progress in Physics*, vol. 76, no. 10, Article ID 106502, 2013.

[2] P. Tonui, S. Oseni, G. Sharma, Q. Yan, and G. Tessema Mola, "Perovskites photovoltaic solar cells: an overview of current status," *Renewable and Sustainable Energy Reviews*, vol. 91, pp. 1025–1044, 2018.

[3] S. Olaleru, J. K. Kirui, D. Wamwangi, K. T. Roro, and B. Mwakikunga, "Perovskite solar cells: the new epoch in photovoltaics," *Solar Energy*, vol. 196, pp. 295–309, 2020.

[4] L. Zhang, J. Miao, J. Li, and Q. Li, "Halide perovskite materials for energy storage applications," *Advanced Functional Materials*, vol. 30, no. 40, Article ID 2003653, 2020.

[5] J. Kim, K.-W. Seo, S. Lee, K. Kim, C. Kim, and J.-Y. Lee, "All-in-One process for color tuning and patterning of perovskite quantum dot light-emitting diodes," *Advanced Science*, vol. 9, no. 13, Article ID 2200073, 2022.

[6] Y. Chen, L. Zhang, Y. Zhang, H. Gao, and H. Yan, "Large-area perovskite solar cells – a review of recent progress and issues," *RSC Advances*, vol. 8, no. 19, pp. 10489–10508, 2018.

[7] P. Roy, N. Kumar Sinha, S. Tiwari, and A. Khare, "A review on perovskite solar cells: evolution of architecture, fabrication techniques, commercialization issues and status," *Solar Energy*, vol. 198, pp. 665–688, 2020.

[8] National Renewable Energy Laboratory, *Best Research-Cell Efficiency*, National Renewable Energy Laboratory, Colorado, 2022.

[9] L. P. Lekesi, L. F. Koao, S. V. Motloung, T. E. Motaung, and T. Malevu, "Developments on perovskite solar cells (PSCs): a critical review," *Applied Sciences*, vol. 12, pp. 672–2, 2022.

[10] Y. Rong, Y. Hu, A. Mei et al., "Challenges for commercializing perovskite solar cells," *Science*, vol. 361, no. 6408, pp. 09–21 2018, Article ID eaat8235, 2018.

[11] K. Moore and W. Wei, "Applications of carbon nanomaterials in perovskite solar cells for solar energy conversion," *Nano Materials Science*, vol. 3, no. 3, pp. 276–290, 2021.

[12] P. Pradid, K. Sanglee, N. Thongprong, and S. Chuangchote, "Carbon electrodes in perovskite photovoltaics," *Materials*, vol. 14, no. 20, pp. 10–12, 2021.

[13] S. Gao, X. Zhao, Q. Fu et al., "Highly transmitted silver nanowires-SWCNTs conductive flexible film by nested density structure and aluminum-doped zinc oxide capping layer for flexible amorphous silicon solar cells," *Journal of Materials Science & Technology*, vol. 126, pp. 152–160, 2022.

[14] M. Hadadian, J.-H. Smått, and J.-P. Correa-Baena, "The role of carbon-based materials in enhancing the stability of perovskite solar cells," *Energy & Environmental Science*, vol. 13, no. 5, pp. 1377–1407, 2020.

[15] S. S. Mali, H. Kim, H. H. Kim, G. R. Park, S. E. Shim, and C. K. Hong, "Large area, waterproof, air stable and cost effective efficient perovskite solar cells through modified carbon hole extraction layer," *Materials Today Chemistry*, vol. 4, pp. 53–63, 2017.

[16] V. Babu, R. Fuentes Pineda, T. Ahmad et al., "Improved stability of inverted and flexible perovskite solar cells with carbon electrode," *ACS Applied Energy Materials*, vol. 3, no. 6, pp. 5126–5134, 2020.

[17] Z. Ku, Y. Rong, M. Xu, T. Liu, and H. Han, "Full printable processed mesoscopic CH3NH3PbI3/TiO2 heterojunction solar cells with carbon counter electrode," *Scientific Reports*, vol. 3, no. 1, p. 3132, 2013.

[18] M. Que, B. Zhang, J. Chen, X. Yin, and S. Yun, "Carbon-based electrodes for perovskite solar cells," *Materials Advances*, vol. 2, no. 17, pp. 5560–5579, 2021.

[19] H. Chen and S. Yang, "Stabilizing and scaling up carbon-based perovskite solar cells," *Journal of Materials Research*, vol. 32, no. 16, pp. 3011–3020, 2017.

[20] Y. Yang, N. D. Pham, D. Yao et al., "Interface engineering to eliminate hysteresis of carbon-based planar heterojunction perovskite solar cells via CuSCN incorporation," *ACS Applied Materials & Interfaces*, vol. 11, no. 31, pp. 28431–28441, 2019.

[21] R. Hu, L. Chu, J. Zhang, X. A. Li, and W. Huang, "Carbon materials for enhancing charge transport in the advancements of perovskite solar cells," *Journal of Power Sources*, vol. 361, pp. 259–275, 2017.

[22] C. Thambiliyagodage and R. Wijesekera, "Ball milling – a green and sustainable technique for the preparation of titanium based materials from ilmenite," *Current Research in Green and Sustainable Chemistry*, vol. 5, Article ID 100236, 2022.

[23] R. Hu, R. Zhang, Y. Ma et al., "Enhanced hole transfer in hole-conductor-free perovskite solar cells via incorporating CuS into carbon electrodes," *Applied Surface Science*, vol. 462, pp. 840–846, 2018.

[24] S. He, L. Qiu, D. Y. Son et al., "Carbon-based electrode engineering boosts the efficiency of all low-temperature-processed perovskite solar cells," *ACS Energy Letters*, vol. 4, no. 9, pp. 2032–2039, 2019.

[25] P. Tonui, S. O. Oseni, G. Sharma, Q. Yan, and G. Tessema Mola, "Perovskites photovoltaic solar cells: an overview of current status," *Renewable and Sustainable Energy Reviews*, vol. 91, pp. 1025–1044, 2018.

[26] S.-T. Zhang, "Study of Fluorine-Doped Tin Oxide (FTO) Thin Films for Photovoltaics Applications," 2017, https://www.theses.fr/2017GREAI021.

[27] N. Poespawati, J. Sulistianto, T. Abuzairi, and R. Purnamaningsih, "Performance and Stability Comparison of Low-Cost Mixed Halide Perovskite Solar Cells: CH3NH3PbI3- x Cl x and CH3NH3PbI3- x SCN x," *International Journal of Photoenergy*, vol. 2020, Article ID 8827917, 10 pages, 2020.

[28] N. Arora, M. I. Dar, A. Hinderhofer et al., "Perovskite solar cells with CuSCN hole extraction layers yield stabilized efficiencies greater than 20%," *Science*, vol. 358, no. 6364, pp. 768–771, 2017.

[29] A. K. Mishra and R. K. Shukla, "Fabrication and characterization of perovskite (CH3NH3PbI3) solar cells," *SN Applied Sciences*, vol. 2, no. 3, p. 321, 2020.

[30] G. B. Mahendran, S. J. Ramalingam, J. B. B. Rayappan, S. Kesavan, T. Periathambi, and N. Nesakumar, "Green preparation of reduced graphene oxide by Bougainvillea glabra flower extract and sensing application," *Journal of Materials Science: Materials in Electronics*, vol. 31, no. 17, pp. 14345–14356, 2020.

[31] O.-E. Plastiras, E. Deliyanni, and V. Samanidou, "Applications of graphene-based nanomaterials in environmental analysis," *Applied Sciences*, vol. 11, no. 7, p. 3028, 2021.

[32] G. W. H. Siti Fauziyah Rahman, "Amperometric detection of dopamine based on a graphene oxide/PEDOT:PSS composite electrode," *International Journal of Technology*, vol. 11, no. 5, pp. 291–319, 2020.

[33] E. Barruna, J. Sulistianto, and N. R. Poespawati, "The effect of CuSCN concentration variations in activated carbon electrode on the perovskite solar cells performance," in *Proceedings of the 2021 17th International Conference on Quality in Research (QIR): International Symposium on Electrical and Computer Engineering*, pp. 1–4, Tamil Nadu, India, June 2021.

[34] A. G. Elang Barruna, R. Muhamad Naufal, M. R. Nugraha et al., "Material characteristics and electrochemical performance of lithium-ion capacitor with activated carbon cathode derived from sugarcane bagasse," *IOP Conference Series: Earth and Environmental Science*, vol. 673, no. 1, p. 12018, 2021.

[35] M. Dwiyaniti, A. G. Elang Barruna, R. Muhamad Naufal, I. Subiyanto, R. Setiabudy, and C. Hudaya, "Extremely high surface area of activated carbon originated from sugarcane bagasse," *IOP Conference Series: Materials Science and Engineering*, vol. 909, no. 1, p. 12018, 2020.

[36] J. He, C. Zou, J. Zhao et al., "Influence of Raman spectroscopy test conditions on the results of carbon chemical structure of chars," *Energies*, vol. 15, pp. 2–15, 2022.

[37] S. Pitchaiya, N. Eswaramoorthy, M. Natarajan et al., "Perovskite solar cells: a porous graphitic carbon based hole transporter/counter electrode material extracted from an invasive plant species Eichhornia crassipes," *Scientific Reports*, vol. 10, no. 1, p. 6835, 2020/04/22 2020.

[38] M. Inagaki, F. Kang, M. Toyoda, and H. Konno, "Chapter 1 introduction," in *Advanced Materials Science and Engineering of Carbon*, M. Inagaki, F. Kang, M. Toyoda, and H. Konno, Eds., Butterworth-Heinemann, Oxford, United Kingdom, 2014.

[39] X. Wu, L. Xie, K. Lin et al., "Efficient and stable carbon-based perovskite solar cells enabled by the inorganic interface of CuSCN and carbon nanotubes," *Journal of Materials Chemistry*, vol. 7, no. 19, pp. 12236–12243, 2019.

[40] L. Mi, Y. Zhang, T. Chen, E. Xu, and Y. Jiang, "Carbon electrode engineering for high efficiency all-inorganic perovskite solar cells," *RSC Advances*, vol. 10, no. 21, pp. 12298–12303, 2020.

[41] A. T. Smith, A. M. LaChance, S. Zeng, B. Liu, and L. Sun, "Synthesis, properties, and applications of graphene oxide/reduced graphene oxide and their nanocomposites," *Nano Materials Science*, vol. 1, no. 1, pp. 31–47, 2019.

[42] F. Lin, X. Tong, Y. Wang, J. Bao, and Z. Wang, "Graphene oxide liquid crystals: synthesis, phase transition, rheological property, and applications in optoelectronics and display," *Nanoscale Research Letters*, vol. 10, no. 1, pp. 11–17, 2015.

[43] W. S. Hummers and R. E. Offeman, "Preparation of graphitic oxide," *Journal of the American Chemical Society*, vol. 80, no. 6, p. 1339, 1958.

[44] U. Ritter, P. Scharff, C. Siegmund et al., "Radiation damage to multi-walled carbon nanotubes and their Raman vibrational modes," *Carbon*, vol. 44, no. 13, pp. 2694–2700, 2006.

[45] S. Rawal, B. Joshi, and Y. Kumar, "Synthesis and characterization of activated carbon from the biomass of Saccharum bengalense for electrochemical supercapacitors," *Journal of Energy Storage*, vol. 20, pp. 418–426, 2018.

[46] M. R. Muda, M. M. Ramli, S. S. Mat Isa et al., "Structural and morphological investigation for water-processed graphene oxide/single-walled carbon nanotubes hybrids," *IOP Conference Series: Materials Science and Engineering*, vol. 209, no. 1, Article ID 012030, 2017.

[47] M. V. Ivanova, C. Lamprecht, M. Loureiro, J. Huzil, and M. Foldvari, "Pharmaceutical characterization of solid and dispersed carbon nanotubes as nanoexcipients," *International Journal of Nanomedicine*, vol. 7, pp. 403–415, 2012.

[48] S. Suragtkhuu, O. Tserendavag, U. Vandandoo et al., "Efficiency and stability enhancement of perovskite solar cells using reduced graphene oxide derived from earth-abundant natural graphite," *RSC Advances*, vol. 10, no. 15, pp. 9133–9139, 2020.

[49] S. Fang, D. Huang, R. Lv et al., "Three-dimensional reduced graphene oxide powder for efficient microwave absorption in the S-band (2–4 GHz)," *RSC Advances*, vol. 7, no. 41, pp. 25773–25779, 2017.

[50] B. Zong, W. Fu, Z. Guo et al., "Highly stable hole-conductor-free perovskite solar cells based upon ammonium chloride and a carbon electrode," *Journal of Colloid and Interface Science*, vol. 540, pp. 315–321, 2019.

[51] P. Kajal, J. H. Lew, A. Kanwat et al., "Unveiling the role of carbon black in printable mesoscopic perovskite solar cells," *Journal of Power Sources*, vol. 501, Article ID 230019, 2021.

[52] C. Punckt, F. Muckel, S. Wolff et al., "The effect of degree of reduction on the electrical properties of functionalized graphene sheets," *Applied Physics Letters*, vol. 102, no. 2, pp. 23114–23118, 2013.

[53] D. Bogachuk, S. Zouhair, K. Wojciechowski et al., "Low-temperature carbon-based electrodes in perovskite solar cells," *Energy & Environmental Science*, vol. 13, no. 11, pp. 3880–3916, 2020.

[54] Y. Omar, C. Maragliano, C. Y. Lai et al., "Multi-wall carbon nanostructured paper: characterization and potential applications definition," *Materials Research Express*, vol. 2, no. 9, Article ID 095601, 2015.

[55] M. Sabry and A. E. Ghitas, "Influence of temperature on methods for determining silicon solar cell series resistance," *Journal of Solar Energy Engineering*, vol. 129, no. 3, pp. 331–335, 2007.

[56] J. Wang, J. Li, X. Xu, Z. Bi, G. Xu, and H. Shen, "Promising photovoltaic application of multi-walled carbon nanotubes in perovskites solar cells for retarding recombination," *RSC Advances*, vol. 6, no. 48, pp. 42413–42420, 2016.

[57] E. Barruna, A. Saniah, R. Bhaskara, S. F. Rahman, A. Zulfia, and N. R. Poespawati, "Carbon nanotubes, graphite, and reduced graphene oxide in CuSCN incorporated carbon electrodes in perovskite solar cells," in *Proceedings of the 2022 11th Electrical Power, Electronics, Communications, Control, and Informatics Seminar*, pp. 23–25, IEEE, Malang, East Java, Indonesia, August 2022.

[58] Y. Cai, L. Liang, and P. Gao, "Promise of commercialization: carbon materials for low-cost perovskite solar cells," *Chinese Physics B*, vol. 27, no. 1, Article ID 018805, 2018.